KryptoJelly: A Jellyfish Robot with Confined, Adjustable Pre-stress, and Easily Replaceable Shape Memory Alloy NiTi Actuators

Yara Almubarak[1], Matthew Punnoose[1], Nicole Xiu Maly[1], Armita Hamidi[1], and Yonas Tadesse[1]

[1]Humanoid, Biorobotics and Smart Systems (HBS) Laboratory, Mechanical Engineering Department, Jonsson School, The University of Texas at Dallas, Richardson, TX, USA.

***Corresponding Author:**
Yonas Tadesse
Yonas.tadesse@utdallas.edu

Abstract

Exploring the world beneath the ocean has been a difficult task, especially in depths that are unsafe for humans. Studying underwater creatures can be very sensitive due to disturbances resulting from typical remotely operated vehicles (ROVs) currently used. Soft robots consist of elastomeric materials, compliant actuators, sensors and other supporting structures, which enable them to be used for numerous applications due to their flexibility, light weight, low noise, and many degrees of freedom. Mechanical actuators, such as pneumatic actuators and servomotors, introduce design constraints related to their size, weight, and cost. Moreover, vibration and noise are undesired attributes that preclude the use of robots developed with such technologies and might disturb the test environment. This paper presents a robust design of a jellyfish-like robot with eight bell segments, named KryptoJelly. The presented robot can perform multidirectional swimming by NiTi shape memory alloys (SMA) actuators confined in a conduit and activated by electrical current stimulation. KryptoJelly is constructed from a 3D printed rigid structure and a soft silicone bell that closely mimics the biological locomotion and appearance of a jellyfish found in nature; the *Chrysaora colorata* species. Four 127 μm diameter SMA wires (of mass 14 mg each) were used per channel to deform the silicone bell margin. The robot can operate up to 1608 cycles continuously for 1.5 hours underwater at high power input (3 times higher than the standard) and sustain its own total body mass of 650 g (~6,000 times the weight of the actuators used). KryptoJelly is able to maneuver in both vertical and horizontal directions during bell contraction-expansion cycles. A study on the effect of multistage-power-time input sequence of NITi SMA actuators and bell design, which results in swimming, is presented. This work has shown the great potential of employing smart materials in biomimetic soft robots, that can be deployed for eco-friendly underwater exploration or other applications.

Keywords: Underwater robots, shape memory alloys, biomimetic, jellyfish, swimming, multidirectional, soft robot

1. Introduction

The soft robotics field is constantly evolving as researchers frequently work with new materials in order to optimize their performance. The functionality of a soft robot is dependent on its ability to withstand variation in pressure, geometry, temperature, and radiation [1] while also operating at a desired level of performance. The initial motivation of soft robotics is bioinspiration [2], which refers to replicating animals using synthetic materials to illustrate a high degree of freedom robot. The jellyfish is an inspiring underwater creature, which has a soft body consisting of a dome shaped structure and tentacles. The size of the dome and tentacles differs based on the species. For example, the *Aurelia aurita* species, or moon jellyfish, consists of a dome shaped structure and short tentacles while the *Chrysaora* species has a similar dome structure with long tentacles. The round dome controls the locomotion of the jellyfish; allowing it to move in a desired direction when it contracts as a result of jet propulsion motion or rowing motion, as explained by Colin and Costello [3]. Figure 1 (a) shows, a purple striped jellyfish (scientific name, *Chrysaora)* species, which will be the focus of this paper and the model used for bioinspiration for our robot (also shown in Supplementary Movie 1). The tentacles of the natural jellyfish are used as tools to capture food. Jellyfish are efficient swimmers and

are capable of swimming long distances while exerting low energy, using simple structures, and carrying payloads. The combination of these aspects makes the jellyfish an appropriate inspiring candidate for designing low profile, low maintenance surveillance and exploration robots. The simplicity and functionality of the swimming biomechanics of these underwater creatures have inspired researchers to study and deploy similar swimming structures in robots [4]. Employing lightweight artificial muscles enables the use of additional sensors and exploration devices on the robots, which makes them intelligent. These robots have the potential to be used in archaeology, the oil industry, the military or even collecting seafood in harsh shallow water environments when combined with soft manipulators [5]. Underwater robots can perform certain tasks that humans are typically unable to accomplish due to size constraints or high-risk environments. The use of noiseless actuators brings a huge advantage compared to the typical motors which can disturb the environment. Monitoring new sea creatures in their natural habitat and exploring, calls for low profile and low disturbances of the environment, which conventional mechanical components are incapable of maintaining at the same level as smart actuators.

In this paper, we present a multidirectional swimming jellyfish robot named KryptoJelly shown in Figure 1 (b-e) that is capable of swimming up to speeds of 60 mm/s. Vertical and horizontal swimming are shown in Movie 2-3 respectively while carrying a payload of 650g of its own 3D printed actuator housing and silicone bell. Multidirectional underwater locomotion by a jellyfish like robot carrying a payload is not presented in prior literature. Figure 1 (d and e) show detailed snapshots of the bell's full contraction sequence at the first heating instance (duration of 0.7s). In both vertical and horizontal swimming cases, the jellyfish was able to travel a significant distance of ~15-20 mm for one cycle. The jellyfish inspired locomotion is achieved using NiTi shape memory (SMA) actuators that are integrated in the rigid structure of the robot-hollow 3D printed tubes. KryptoJelly can continuously operate for 1608 cycles underwater at a power 3 times higher than the standard power recommended by the manufacturer (Dynalloy Inc.). In the jellyfish design shown in Figure 2 (a), the body consists of a 3D printed rigid structure while the soft bell (diameter of 210 mm and thickness of 5 mm) is made of silicone Ecoflex 00-30. The complete CAD model, sectional view, the spring mechanism, and the pulley systems are shown in Figure 2 (b and c). The SMA actuators (4 SMA wires connected in parallel for each of the 8 channels, length L = 95 mm and diameter D = 127 μm) are connected to the bell mechanism through pulleys. When electrical current is supplied, the SMA muscles contract, therefore activating the mechanical movement of the silicone bell through the pulley systems. This causes a flapping motion of the bell, which creates vortex around the bell and enables the robot to swim.

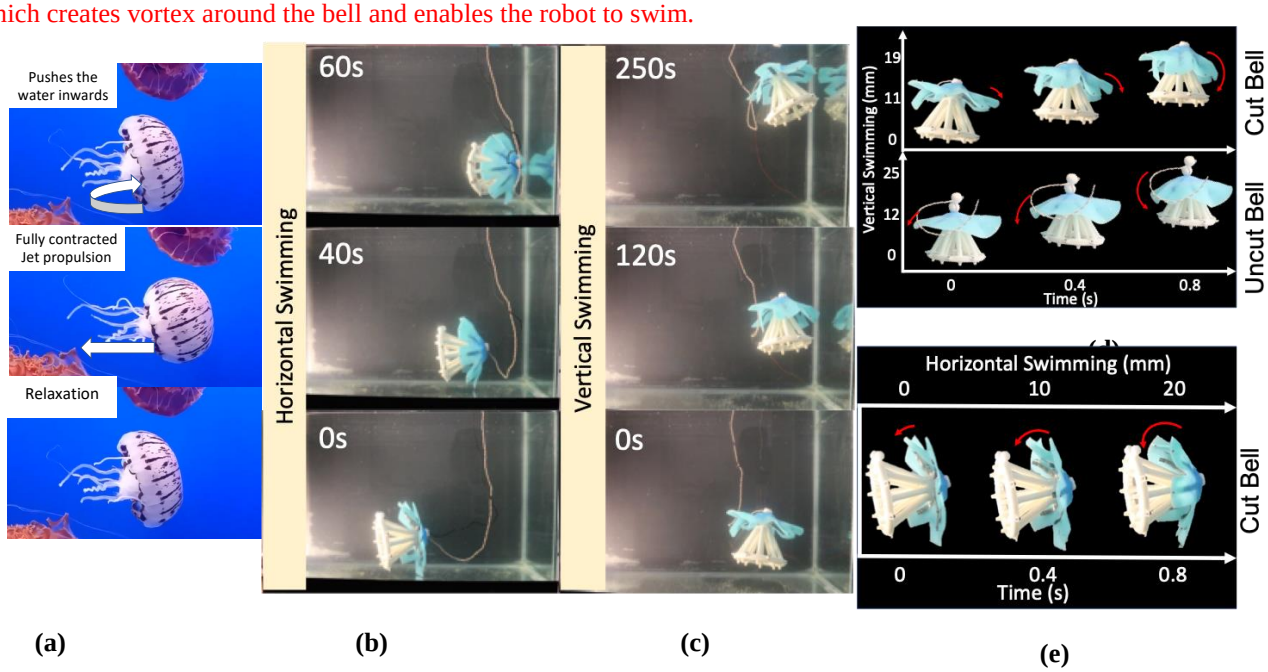

(a) **(b)** **(c)** **(e)**

Figure 1. Jellyfish robot design and insparation: (a) jellyfish found in nature, *Chrysaora colorata* species (stripped-jellyfish), the top picture shows the relaxed mode of the bell before contraction, middle picture shows the contraction of the bell, and the bottom picture shows the relaxation mode, (b) horizontal swimming, and (c) vertical swimming of KryptoJelly, and (d-e) swimming distance versus time at one cycle of the bell deformation for both swimming cases.

The most common material used in soft robotic applications is platinum-cured silicone. This type of silicone can be found in current projects for soft robotics, such as a soft robot capable of forming into different shapes [6], underwater jellyfish [7], biomimetic fish [8], octopus like soft arms [9] and a musculoskeletal joint [10]. Starting in liquid form, the silicone is mixed, allowed to cure at room temperature, and then hardens into the shape of the mold chosen by the designer. Its molding capabilities, flexibility, strength, and durability make this kind of silicone an ideal material for robotic and orthotic applications. Soft robot development requires improvements in the locomotion method, soft actuating technology, and control strategy. Because the method of actuation varies between robots, selecting an actuator that is compatible with the structure and can accomplish the defined tasks efficiently is critical to the success of the robot. This part in the development stage can be difficult, but it is crucial, as each actuator has its own advantages and disadvantages. While electrical motors are energy efficient and easily controlled, they tend to be bulky and expensive. Pneumatic actuators are also not practical in real-world applications because they require an air pump to operate. Researchers today have begun to move towards smart actuators; leaving behind traditional motors and pistons. Smart actuators, such as piezoelectric actuators, ionic polymer-metal composites (IMPCs), dielectric elastomers (DE), twisted and coiled polymer muscles (TCP), and shape memory alloys (SMAs), have shown the capabilities of producing the desired actuation with adequate performance, extremely quiet operation, and compact size. For instance, the high specific power of SMAs allows them to be used in applications where compactness is critical [2]. Unfortunately, these actuators would still require a higher input power and are in some cases more expensive.

Current developments in underwater robotics are presented in several papers where utilizing smart materials is shown as the major part of the work. A bionic jellyfish based on tissue engineering is presented in [11]. A micro-robotic fish [12] is demonstrated, which moves based on an actuated biomimetic fin that contained an elastic substrate embedded with SMA wires. In another study, an undulating eel robot is made of a flexible polyurethane [13]. Similarly, a robotic jellyfish, Robojelly [7], is created after gaining inspiration from the *Aurelia Aurita* species found in nature. This underwater robot uses shape memory alloy embedded in a bio-inspired RTV silicone bell in order to mimic the typical structure of the species. A hydrogen and oxygen fuel-powered jellyfish model is also proposed in [14], using nickel-titanium, multiwall carbon nanotube, and nano-platinum (NiTi/MWCNT/Pt) composite actuators, in order to imitate the ordinary movement of a jellyfish. The jellyfish like robot in Villanueva et al. 2011 [7] is based on the species Aurelia aurita (Moon jellyfish), whereas our current work in this paper (Figure 1) is based on the species *Chrysaora colorata* species (stripped-jellyfish, Figure.1 (a)). The *Aurelia aurita* has very short tentacles under the dome-like bell, whereas *Chrysaora* has long tentacles. The unique oral arms of this species (*Chrysaora*) closely match to the bioinspired jellyfish robot presented here, a robot having actuators configured around the bell in distinct hollow channels. However, in our design, we used a rigid structure to house the actuators and they are not flexible oral arms as the natural counterpart. We did not try to mimic the entire anatomy of the jellyfish, but we tried to mimic certain parts of the animals for bioinspiration. Similar hollow channel design of a jellyfish was presented in Tadesse et al 2012 [14], but the focus of that work was on powering using hydrogen fuel, not swimming performance.

In addition, a biomimetic jellyfish robot is developed implementing IPMC actuators [15]. In many instances, the jellyfish design concept demonstrated desired characteristics, such as JenniFish [16] which uses fluidic actuators, the PiezoMEMS actuated robotic jellyfish [17], the untethered soft jellyfish presented in [18] actuated using dielectric elastomer, and jetPRO robotic jellyfish presented in [19] actuated by a mechanical iris diaphragm that create propulsion due to volumetric change within the system. FludoJelly is one of the fastest jellyfish-like robot that can reach swimming speeds up to 160 mm/s while carrying a payload of 100 g mass. However, it is not actuated by smart materials [20]. Other jellyfish models using smart actuators include robotic jellyfish using DEs [21], using coiled SMA springs [22], and the jellyfish robot based on a smart modular structure (SMA/ PDMS/PVC composite) [23] show promising results in the field of underwater soft robotics specifically on jellyfish. Other advances in underwater robotics that have been introduced are the lamprey-based undulatory vehicle [24], free-swimming robotic batoid ray with IPMC actuators [25], and the propulsion-induced miniature fish-like swimmer generated by tail vibrations [26]. Even more recently, a robotic fish developed with 3D printing and an electromagnetic actuation system is presented in [27]. Chu et al.[28] has shown extensive literature on the application of smart materials such as SMA, IPMC, and PZT for underwater robots. We will not focus on all underwater soft robots in this paper to narrow down the scope. However, Salazar et al. [29, 30] have shown several underwater robots and extensive literature. Table 1 shows a comparison of related jellyfish swimming robots actuated by smart materials and the fastest from literature and the one presented in this paper.

The highlights of this work can be summarized as:

- A biomimetic jellyfish robot is designed and developed using SMAs as artificial muscles in order to mimic the behavior of the real jellyfish for efficient swimming. In this design, 4 SMA wires are connected in parallel and each set is confined in the 8 channels under the jellyfish bell with uniform thickness. Therefore, the actuators are easily adjustable, replaceable and this architecture makes the design robust. The design, integration process and swimming are explained in Figure 1 and Figure 2
- Successful multidirectional underwater maneuvering of KryptoJelly while carrying a payload of 650g (6,000 times the weight of its SMA actuators) of 3D printed structure and silicone bell is performed as shown in Figure 2.
- Full characterization of NiTi SMA actuators as well as lifecycle testing of SMA at high power in underwater condition is presented. The performance of the SMA by 2-step and 5-step high power input at three different pre-stress loads are compared (Figure 3). Decreasing the input power gradually, increases the duration of the actuated state, which helps the robot have more efficient swimming.
- Endurance test of the robot for cyclic actuation in underwater (1 hour and 33 minutes) at high power input (5-step power input mode) while connected to a power supply was determined, as shown in Figure 4.
- The robot achieves an instantaneous swimming speed up to 60 mm/s (vertical swimming) and 45 mm/s (horizontal swimming). The vertical speed of KryptoJelly is highest among other presented jellyfish robots used non-conventional actuators (table 1). The effect of varying bell configuration on swimming is studied and presented in Figure 5 and Figure 6.

To begin, this paper reviews related works, followed by a discussion on the design, fabrication, and actuator integration of KryptoJelly. The paper then continues with underwater actuation characterization of the NiTi actuator, lifecycle testing, a swimming analysis of KryptoJelly and untethered swimming experiments. Finally, the conclusion and future works are presented.

Table 1: Comparison of swimming jellyfish robots presented in the literature.

Paper	Actuator	Wireless controllability	Voltage (V)	Current (A)	Power (W)	Frequency (Hz)	Weight (g)	Bell Diameter (mm)	Velocity (mm/s) V: vertical H: horizontal
RoboJelly [7]	SMA wire	No	-	1.5	~100	0.5	242	164	V: 50
JenniFish [16]	PneuNet	Yes	-	-	2.29-5.85	0.8-0.435	380	210	V: 30
DE Jellyfish [21]	Dielectric Elastomer	No	6000	-	-	-	270	-	V: 10
Modular Jellyfish [23]	SMA wire	Yes	-	1	-	0.5	-	216	V: 45
Untethered Jellyfish [18]	Dielectric Elastomer	Yes	7000-9000	-	-	1.6	28	156	V:5-10
Synthetic Jellyfish [22]	Coiled SMA spring	No	18-19	-	104-115	0.5	-	76	-
JetPRO [19]	Micro DC gear Motor	No	10	-	-	-	80	30	V:116
FludoJelly [20]	Pneumatic (Air)	No	12	-	-	0.8	500	220	V: 160
KryptoJelly (this paper)	SMA wire	Yes	12	30	~360	0.33	650*	210	V= 60 H:45

* 650(600g of 3D printed body, 50g of silicone bell). Not considering electrical component.

2. Materials and Methods

2.1. Design and Fabrication

The design of the jellyfish robot is inspired by real jellyfish found in nature, as shown in Figure 1 (a). This was based on the prior work done on the hydrogen fuel powered jellyfish [14]. As shown in the detailed CAD design in Figure 2 (a-c), the 3D printed design consists of eight hollow tubes (channels) that house the SMA actuators. An internal housing at the center contains the mechanical pulley unit (Figure 2(b)). Each actuator controls 1/8th of the soft silicone bell structure. The jellyfish is fabricated using several steps. First, the pulleys are connected to each of the 8 sections as shown in the pulley assembly section in Figure 2(b). Second, the spring steels are connected to the rigid structure. The spring steels are used to help the silicone bell return back to its original position after actuation. The bending of the spring steels helps create a smooth curvature on the silicone bell, mimicking the natural look of the jellyfish. A circular plate with a 210 mm diameter and 5 mm thickness was used to mold the bell. 250 ml of mixed platinum cured silicone Ecoflex 00-30 (1:1 mixture of part A & B) was poured to produce the soft bell. EcoFlex 00-30 (Smooth-On-Inc.) has a shore hardness of 00-30 and up to 900% elongation at break, a tensile strength of 200 psi (1379 kPa), pot life of 45 minutes, and a curing time of 4 hours at room temperature (23 ^{o}C) [24]. A coloring agent, Silc Pig color (Smooth-On-Inc.) is used for aesthetic purposes without affecting the performance of the bell. After curing, the cast silicone bell can be cut to the desired bell geometry or kept as it is and mounted on the spring steels.

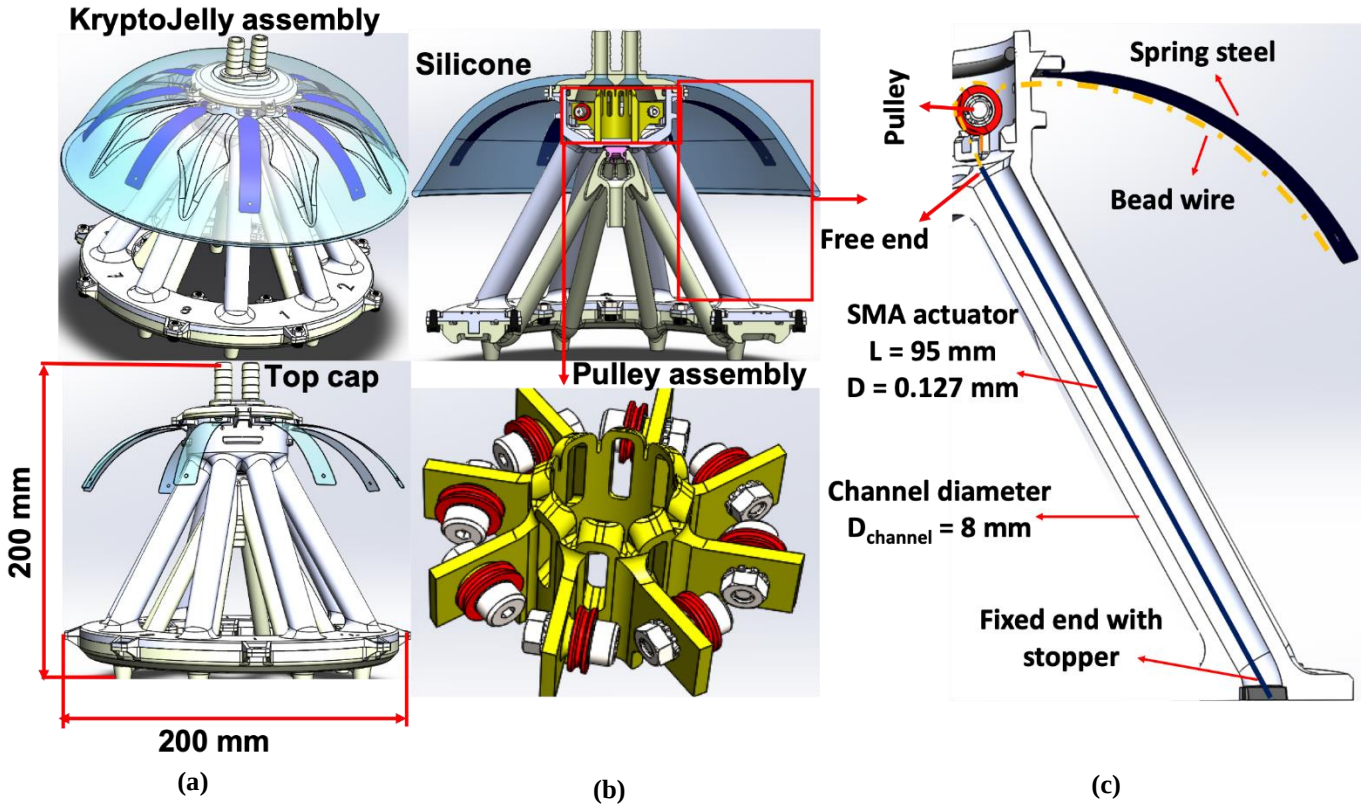

Figure 2. Design and assembly of KryptoJelly: (a) CAD design of the robot showing major components and assembly of the jellyfish robot, (b) sectional view and detailed pulley assembly, (c) a detailed sectional view of actuator connection in a channel that can be used to easily replace actuators or cooling.

2.2. Actuator Integration

The rigid structures of KryptoJelly (the hollow channels) are used to house the actuators (Figure 2(c)). The actuators in this design can be replaced easily if damaged, if one wants to change the number of actuators within a channel, or to adjust the pre-stress level of the actuators. The silicone dome-like structure and the integrated spring steel can be kept intact and can be used multiple times. As these components do not fail after several actuation cycles. The most vulnerable parts that fail during testing of the jellyfish are the actuators, which need constant replacement. Therefore, the ability of changing the actuators makes our design robust. This unique feature is important, as it does not limit the jellyfish-like robot to be tested in one actuation parameter. Using this method, the SMA can be easily adjusted for pre-tensioned and replaced if damaged. Furthermore, the channels are provisions for cooling actuators, because thermal actuators such as SMAs need active cooling to improve their actuation frequency. However, we will not discuss on active cooling in this paper to limit the scope. The muscle integration process consists of four steps. For actuating each bell, 4 SMA wires of equal geometry (length L = 95mm, diameter D = 127 µm) are used in parallel by initially crimping them together. Then, an actuator end stopper is added at one end, and copper wires are soldered to the crimps connected on both ends of the actuator. Third, a bead wire is passed through guides, which are fixed on the spring steels and connected to the SMA muscles through the pulleys. Fourth, the SMA is fed into the hollow tube. Finally, the bead wire is tied to the tip of the spring steel (shown in sectional view in Figure 2 (c)) with an optimal pre-stress of 300 g, which was determined from the muscle characterization results presented in a later section of the paper. Using this integration method, the SMA is fixed at the bottom end and actuated linearly by pulling the bead wire and causing the silicone bell to move. Positioning the actuator inside the hollow tubes rather than embedding it directly in the silicone similar to works presented in [7] increases the accessibility in changing the design and studying the performance of the jellyfish under different actuator parameters such as varying the wire diameter, pretension, and the number of actuators in each channel. When the actuator is integrated utilizing the process used for KryptoJelly, it can be easily replaced if damaged. Also, the hollow tube allows a small amount of water or fluid to be confined around the actuator for active cooling and actuation performance enhancement. All the mentioned properties make our prototype robust in design.

3. Results and Discussion

3.1. Shape Memory Alloys (NiTi) and Muscle Characterization

To understand the material properties of the SMA actuators that drive KryptoJelly, characterization tests were done. Our aim in this section is to study the parameters of the actuator that are useful for swimming and not to characterize the SMA entirely. Shape memory alloys are known for their muscle-like actuation, lightness in weight, high power density to weight ratio, and simple voltage control. At standard power inputs recommended by the manufacturer, the actuator can achieve a total strain of 4% of its loaded length. These smart materials can actuate due to phase transformation resulting from the change of temperature and applied stress. However, they demonstrate large hysteresis due to their non-linear strain response. As a result, active cooling is highly recommended to improve the performance. Actuating in a fluid medium such as water plays a vital role in increasing the actuation frequency and lowering the temperature response due to the active cooling phenomena [31]. Extensive studies have been conducted to study the effect of pre-stress and actuation frequency [32]. Furst and Seelecke [33] show a relation between the power density, pre-stress, and actuation frequency on the performance of the actuators. Song et al. [34] increased the actuation speed of SMA up to 35 Hz by a novel design, using multiple thin SMA wires and sequential actuation. They used resonance phenomena to realize large deformations up to 35 Hz. Konh et al. [35] heated SMA wires by joule heating method via a defined step function. In all of the above, SMAs are great for certain applications, as their frequency and cooling time are related to each other. In the presented work here, experimental characterization was performed on the SMA in an underwater environment (4 SMAs connected in parallel, length L = 95 mm, diameter D = 127 µm, the total resistance is R = 3.17 Ω). Schematics of the experimental setup are shown in Figure 3(a). The setup included the NiTi SMA actuators shown in Figure 3(b), NI 9221 to measure the voltage, NI 9219 to measure the temperature change using connected thermocouples, and a laptop for measuring and saving the data using LabVIEW program. An open source program called “Tracker” was used to track the displacement of the muscle while actuating underwater, which was captured using a standard video camera. Input current, output voltage, and output temperature versus time were collected at a rate of 100Hz data sampling. The video analysis for measuring the strain was conducted at a rate of 60 fps. All the data were then plotted using MATLAB. The tested samples were identical to the actuators integrated within the jellyfish robot. The SMA actuator parameters are shown in table 2. Three tests of varying pre-stress (100g, 300g, and 500g) were conducted at 2 different power input sequences at an equal heating

frequency of 0.33Hz (duty cycle 66%). The tests consisted of two waveforms (power steps). One of them had two heating steps followed by a cooling step. The second one had five heating steps followed by one cooling step. Figure 3(c) shows the schematics of input current versus time for both power steps. The results are plotted in Figure 3, where Figure 3(d and g) are the strain, Figure 3(e and h) are the temperature, and Figure 3(f and i) are the output voltage for the 2-step and 5-step power input, respectively.

The 2-step power input produced an average strain of 1% for 100 g pre-stress and an average maximum actuation strain of 2.5% at a pre-stress of 300 g and 500 g. On the other hand, the 5-step power input shows an average actuation strain of 2% at 100g pre-stress and almost 4% at both 300 g and 500 g pre-stress. In both power input cases, a bias is observed at the two higher pre-stress values, which can be seen in the heating and cooling cycles in the temperature plot. The bias in all the plots indicates that there is remnant heat in the SMA and the cooling time is short. By comparing the 2-step and 5-step heating power input, it is observed that in underwater condition, the strain has almost doubled as shown in Figures 3 (d and g). Moreover, the 5-step power input allows the actuator to reach higher actuation temperatures (up to 70 ^{o}C in underwater condition). The energy equation (E = P*t) can be used to calculate the energy consumption using the two different power inputs where P is the power [W] and t is the heating time [s]. Using the energy equation, we found that the heating energy in the 2-step powering is lower than the one produced in the 5-step power input (28.5 J compared to 46.75 J), which is consistent with the relation of the increase of area under the power curve for the 5-step power input compared to the other. By observing the actuation results, it is shown that the performance of the SMA actuator is highly dependent on the input current and the duration of the applied current, as well as the initial pre-stress applied on the actuator. The observed bias is indicative that higher cooling times are needed (more than 1s cooling). In this soft robotic application, an increase of energy is required in order to achieve an asymmetric actuation pattern that is a desired performance attribute of the jellyfish. Therefore, the 5-step heating process is the most ideal solution in order to maintain the strain level and the integrity of the actuator. Maintaining the strain for longer times helps the KryptoJelly to have more efficient swimming by pushing and keeping the fluid against the underside of the bell. The power step includes a series of pulses that decrease both in time interval and power to make sure the actuator does not overheat and burn. Although the increase of energy can be a drawback, some solutions can be taken in the future in order to increase efficiency such as pulsed actuation [36], and a locking mechanism [37] which can be used to improve and conserve energy.

Table 2: Properties of NiTi SMA under square wave power input (4 wires connected in parallel used in KryptoJelly)

Material	NiTi Nickle Titanium	
Type of actuation	Electrothermal	
Wire diameter (single SMA wire)	D_1 = 127 µm	
Length of wire	L = 95 mm	
Mass (4 SMA, without crimps)	M = 1.4x10^{-5} kg	
Resistance (4 wires in parallel)	R_4 = 3.17 Ω	
Power (4 wires in parallel)	High Power	Low Power
Current (Input for 4 SMA in parallel)	I = 3.75A	I = 1.3A
Voltage (output for 4 SMA in parallel)	V = 11.88V	V = 4.12V
Actuation power (for 4 SMA in parallel)	P = 44.55W	P = 5.35W
Heating time	t_h = 0.7s	t_h = 1.5s
Cooling time	t_c = 1s	t_c = 10s
Heating energy (for 4 SMA in parallel)	E_h= 31.18J	E_h= 8.025J
Actuation frequency	f = 0.58Hz	f = 0.08Hz
Actuation strain, at 300g load (experimentally)	ε = 4%	ε = 2.5%
Lifecycle (at the high power) 3 times higher than the standard	1608 cycles (1 hour and 33 minutes)	
Blocking force (experimentally)	~ 9 N	
Free strain (experimentally) at power 3 times higher than the standard	4%	

The actuator temperature rise can be predicted using the following simplified heat transfer model as shown in Equation (1) [38]. The actual model may be more complicated than this due to flow conditions.

$$mC_p \frac{dT}{dt} = i^2R - h_cA_c[T(t) - T_\infty] \quad (1)$$

Where *m* is the mass, C_p is the specific heat capacity of the SMA, *T(t)* is the temperature of the SMA at a specific time *t*, T_∞ is the ambient room temperature, *i* is the electrical current, *R* is the resistance of the SMA, h_c is the convective heat transfer of water, and A_c is the surface area of the SMA. The left side is the heat rise in the SMA and the right side is the difference between the input (input power) and the heat loss due to convection. The heat transfer equation would help in reducing the need for future experiments by predicting the temperature behavior of the actuator under varying conditions such as input electrical current, change of actuating environment, and change in material properties such as the specific heat capacity C_p and the surface area A_c of the actuator. Equation (1) shows that the heat rise in the SMA will be significantly affected when tested in water as the convective heat transfer coefficient changes. As a result, higher current is needed when actuating in underwater condition.

3.2. Lifecycle Test

In previous related works, it is mentioned that SMA actuators are capable of operating up to hundreds of cycles in air under standard and ideal actuation conditions before showing any reduction in actuation stroke or fatigue [39]. Lagoudas et al. [40] conducted a comprehensive lifecycle study on NiTiCu SMAs and showed that the thermomechanical fatigue life of the actuator is a function of stress, temperature, and material processing. Zhang et al. [41] investigated the effect of frequency on cyclic behavior and low cycle fatigue ($N < 10^4$) of NiTi SMAs. Prior studies presented that as the frequency increases, the fatigue lifetime under strain-controlled loading shows a decreasing trend for all the strain amplitudes. Maletta et al. [42] studied fatigue life of the NiTi sheet under controlled strain. They showed that increasing strain from 0.7% to 4.5%, reduces the number of mechanical cycles from more than 10^5 to lower than 10^3. Calhoun et al. [43] investigated the fatigue life of SMAs under constant stress condition using the critical plane model presented in [44].

In this study, we investigate the performance of the SMA in underwater condition by performing the tests on an actuator integrated in the jellyfish at the 5-step power input. The lifecycle test was conducted on one bell segment as shown in the experimental setup in Figure 4(a) to estimate the lifespan of KryptoJelly underwater. Figure 4(b) shows the strain degradation at each 200 cycle interval. It is observed that a maximum strain of 7% was achieved at the first few hundred cycles and decreased by half at 800^{th} cycle. The experimental data, such as the output voltage using NI 9221 (National Instrument), temperature using NI 9219 by connecting thermocouples, and the actuation strain using the Keyrence laser displacement sensor, were collected and stored on a laptop using LabVIEW program. During the experiment, the structure is fixed within a fish tank and the motion of the bell is translated to the laser sensor, which is fixed and kept out of the water tank connected to a pulley system (Figure 4(a)). The actuator was capable of actuating underwater for 1608 cycles at a frequency of 0.33Hz (a total of 1 hour and 33 minutes of continuous actuation under 2 s heating and 1 s cooling). The power input (input current and output voltage are shown in Figure 4 (c and d)) used for underwater actuation was 3 times higher than the recommended power prescribed by the manufacturer (Dynalloy Inc.). This test is unique and not shown in the literature mentioned above because: (1) it uses the multistep cyclic input for the SMA actuator, (2) the SMA is actuated in underwater and (3) the input power is higher than the standard power when actuating in air. Therefore, the test will be useful for other researchers for other applications. It is important to note that the strain behavior of the actuator degrades with the increase in the number of cycles, as shown in Figure 4(e), eventually causing fatigue failure and the SMA actuator to break. On the other hand, the temperature profile is increasing as the heat is accumulated in the surrounding water close to the actuator as shown in Figure 4(f). At around the 1200^{th} cycle, the thermocouple disconnected from the actuator, and therefore, the temperature data between 1200 to1608^{th} cycles were not recorded.

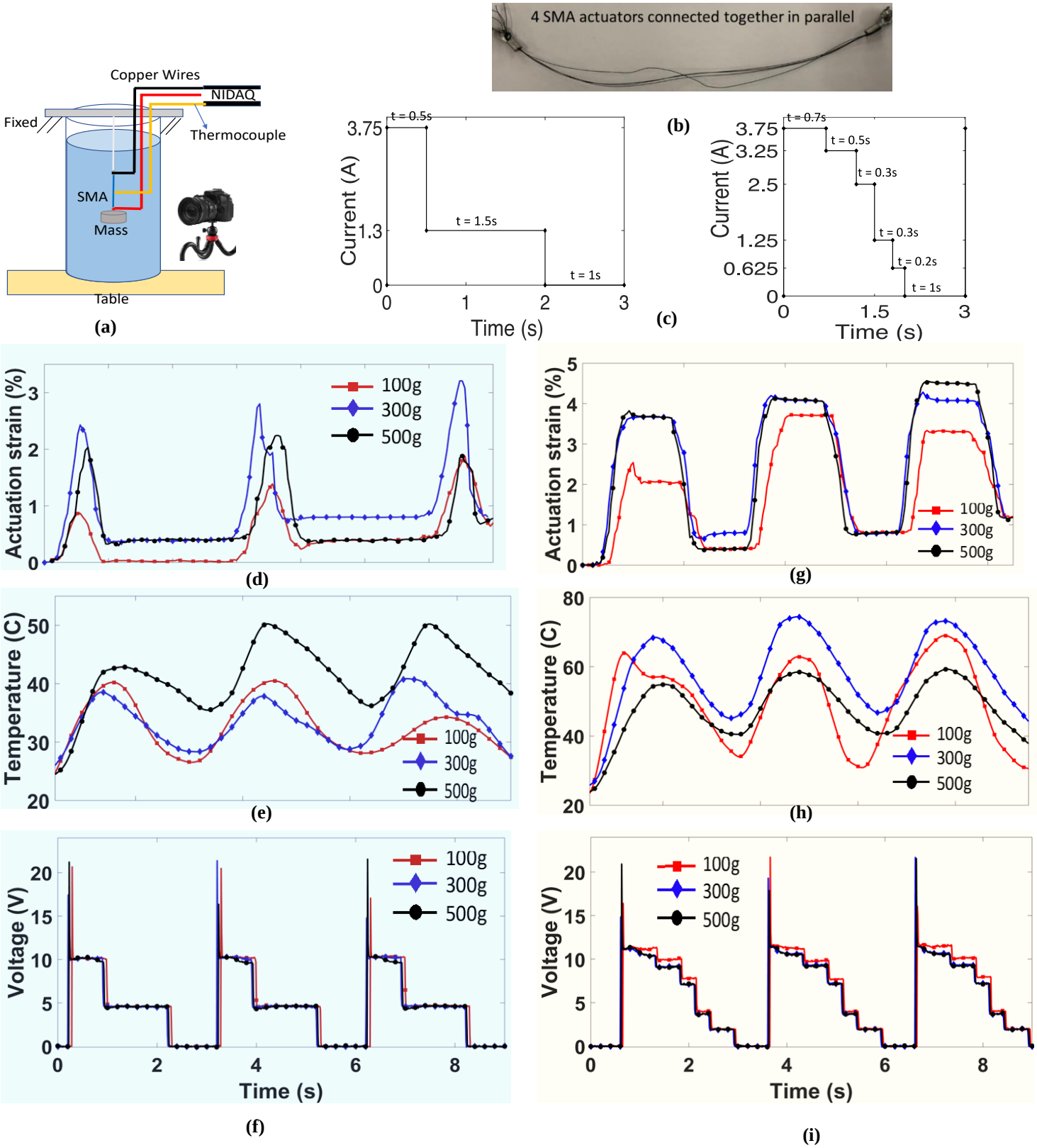

Figure 3. Experimental characterization of SMA actuator in an underwater environment and multistep input sequence: (a) isotonic test experimental setup, (b) snapshot of the muscle sample (4 SMA crimped in parallel) used for the characterization test, (c) current vs time of 2-step power input and 5-step power input. Time-domain plots for 2-step power input: (d) actuation strain, (e) temperature, and (f) output voltage. Time-domain plots for 5-step power input: (g) actuation strain, (h) temperature, and (i) output voltage.

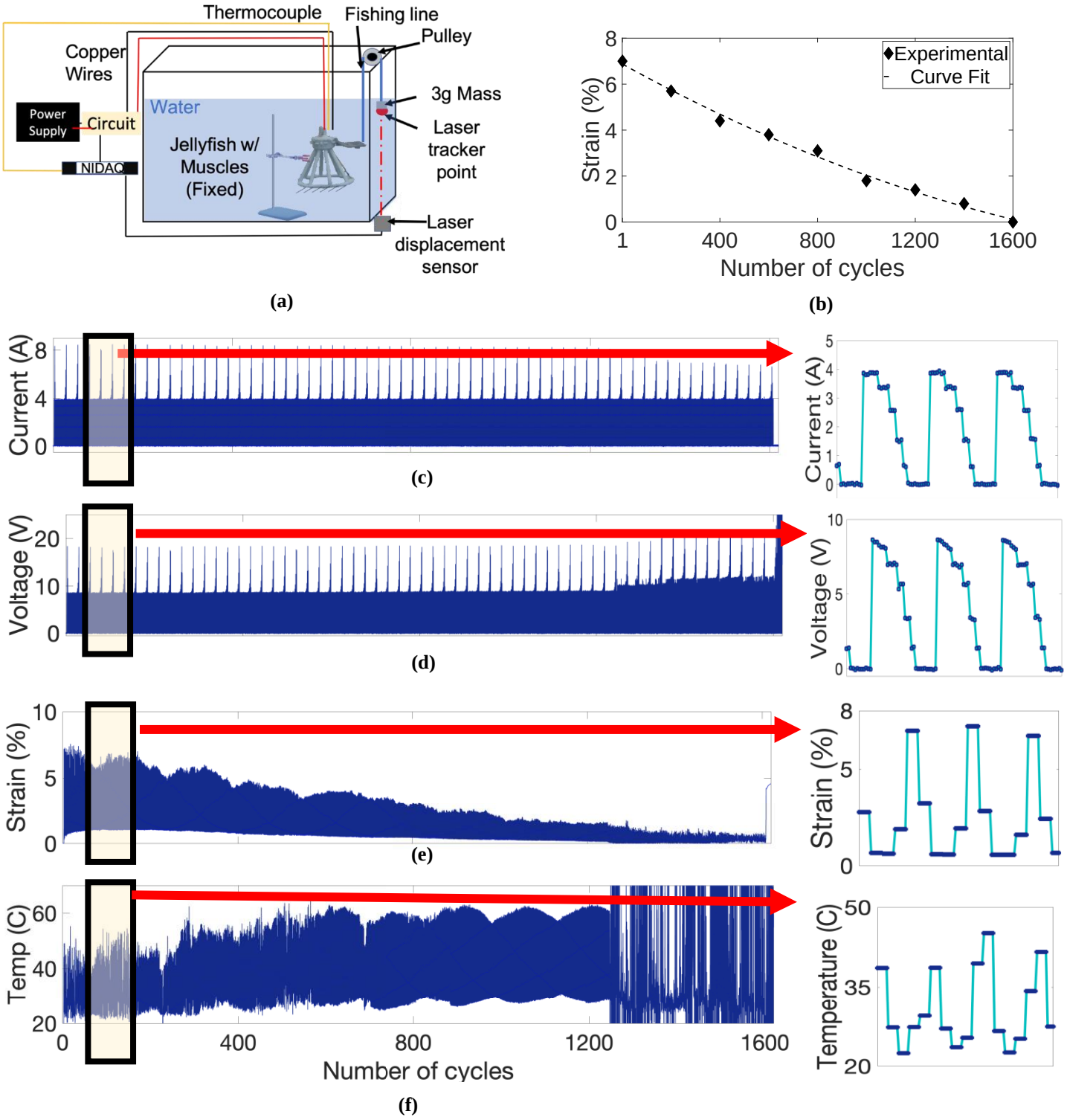

Figure 4. Lifecycle test at high power: (a) schematics of the experimental setup, (b) strain vs lifecycle at 200 cycle intervals. Lifecycle behavior plots of: (c) input current, (d) output voltage, (e) actuation strain, and (f) output temperature.

3.3. Swimming Analysis

3.3.1. Bell Segment Characterization

To better predict and enhance the swimming performance of the bell segment of Kryptojelly, actuation characterization was conducted on the silicone bell at different actuation parameters. The working mechanism of the actuation unit for the silicone bell is shown in Figure 5(a). To examine this mechanism, first, the bending of the bell shown in Figure 5(b) is studied and compared by two different input powering patterns, the 2-step power input versus 5-step power input (Figure 5(c)). In both cases, the maximum input power was 3 times higher than the one recommended by the manufacturer (Dynalloy.Inc). The need for higher power is due to the change in heat transfer parameters when the SMAs are confined in a small channel that is filled with water. Therefore, the SMAs are operating in water, not in air medium as in many previous applications. Considering one of the eight channels, the 2-step current input sequence was given as 3.75 A for 0.5 s followed by 1.3 A for 1.5 s (2 s total ON sequence) and then 0 A for 1 s (OFF sequence). For the 5 steps, the sequence was 3.75 A for 0.7 s, 3.25 A for 0.5 s, 2.5 A for 0.3 s, 1.25 A for 0.3 s, and 0.625 A for 0.2 s (2 s total ON sequence) then 0 A for 1 s (OFF sequence). Figure 5(c) shows the current sequence and bending angle versus time for the two different power inputs. The 5-step power input produced a higher bending angle than the 2-step as a result of increasing the heating energy which is explained in the next section. Second, the segmented versus unsegmented silicone bell are examined to study the effect of it on the swimming of the robot. Figure 5(d) shows the results of the segmented and unsegmented silicone bell using the 5-step power input. It is observed that in the case of a single bell actuation there is no difference in the bending angle whether it is cut or un-cut. When silicone is cast on a mold and directly used as a cover for the bell, it is called an un-cut bell or "unsegmented". On the other hand, if cast silicone is sliced and a triangular region is removed from the periphery, it is referred to as a "cut" bell or "segmented".

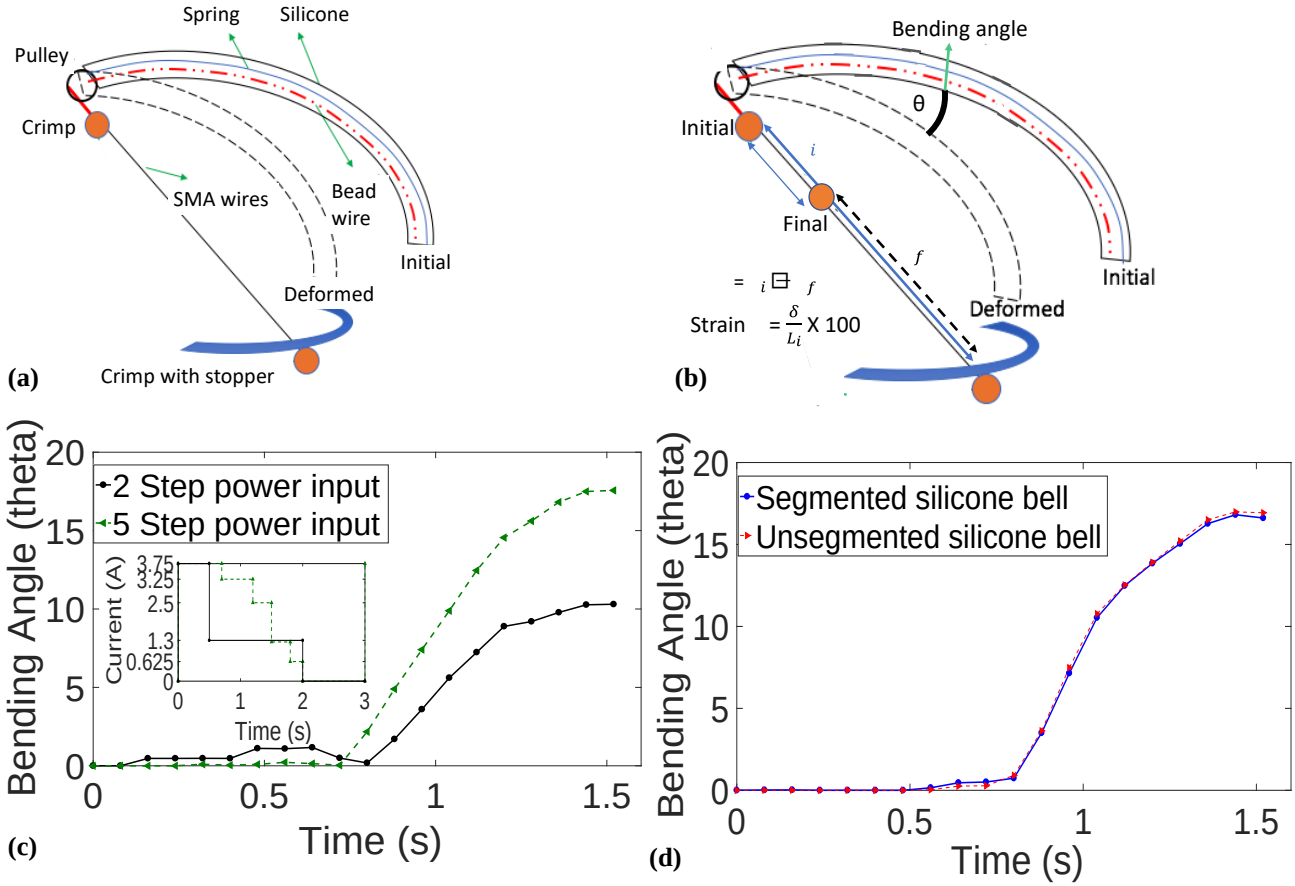

Figure 5. KryptoJelly flapping structure characterization results: (a) Schematic diagram of mechanical connections, (b) schematics of the analyzed bending angle θ, (c) Bending angle versus time for 2 and 5-step power input, (d) Bending angle versus time for segmented and unsegmented silicone bell at 5-step power input.

3.3.2. Swimming Experiments

After completing the design, fabrication, integration and testing one bell segment, discussed in the previous sections, KryptoJelly is deployed in a 70-gallon fish tank for swimming. In each channel, 4 SMA actuators connected in parallel were integrated (length L = 95 mm, total resistance R = 3.17 Ω) with a pre-stress of 300 g. All actuators in the 8 channels were connected in parallel, therefore the 5-step power input was used for testing with the following input current sequence: 30 A for 0.7 s, 26 A for 0.5 s, 20 A for 0.3 s, 10 A for 0.3 s, and 5 A for 0.2 s (2 s total ON heating sequence) then 0 A for 1 s (OFF cooling sequence). The required power was provided by a DC power supply that is connected to the robot. The 30A current was selected based on good actuation (~4 %strain per SMA) that was achieved by several tests conducted on the single bell and was then multiplied by 8 for all the bells. Previous results, Figure 1(d and e) presents snapshots of the jellyfish traveling at the first heating pulse of 30A for 0.7s. In all 3 swimming cases at that short instant, KryptoJelly was traveling at a distance of ~15- 20 mm. Also, KryptoJelly was carrying a payload of almost 650 g of its own 3D printed rigid structure and silicone bell.

Vertical swimming was achieved by testing the two different configurations. One was conducted without cutting the silicone into 8 segments while the other was done after cutting. Unlike the one bell segment characterization, there was a significant difference between swimming performance using a segmented and unsegmented bell. Figure 6(a) shows the vertical swimming versus time for both cases. It is observed that KryptoJelly moved faster when using the solid silicone bell (unsegmented) due to the increase in surface area when flapping. This increase in surface area causes more water volume to retain into the sub-structure, which results in a higher-pressure gradient and water circulation generated around the body. Therefore, the jellyfish moves because of this water pressure gradient. Referring back to Figure 6(a), the unsegmented bell allowed KryptoJelly to travel a distance of 200 mm with a total of ~25 actuation pulses (70 s). On the other hand, the segmented bell enables the jellyfish robot to travel 300 mm with a total of ~84 actuation pulses (250 s). When normalizing the data, in the unsegmented and segmented cases, KryptoJelly was able to travel 8 mm/pulse and 3.5 mm/pulse respectively after completing one actuation cycle (5 heating followed by 1 cooling). The differences in swimming height for the segmented and unsegmented bells is due to different starting points used for both tests. The results of these tests are shown together in order to illustrate the difference in slope of the swimming height versus time. For the unsegmented silicone, the jellyfish can reach an instantaneous swimming velocity of 60 mm/s compared to 51 mm/s for the cut silicone as shown in Figure 6(b). If we study the relation between the number of cycles and the distance travel for both bell configurations, we can estimate that for the first unsegmented configuration, KryptoJelly would be able to travel longer distances at a faster rate (as can be seen in the slope). A fast camera was used to capture the swimming performance at a rate of 100 Hz shown in Supplementary Movie 2.

Horizontal swimming (Movie 3) is also performed at an instantaneous swimming speed of 45 mm/s, shown in Figure 6 (c-d). In this case, the robot was oriented horizontally at one position and actuated. It travelled 350 mm within 70 s (average speed 5 mm/s). In both cases of vertical and horizontal swimming (Figure 6(a and c)) small bumps can be seen in the displacement. When moving vertically, KryptoJelly is swimming against gravity therefore at the relaxed state and due to its own weight, the jellyfish would sink slightly. On the other hand, when moving horizontally as the bell contracts the robot is able to push itself forward, swimming perpendicular to gravity and when it relaxes due to the opposite motion of the bell it would push the structure slightly backward. The focus on actuation frequency and asymmetric actuation presented in Figure 3(g) previously, is highly important to prevent the actuating bell from fully relaxing and returning to its original positions. Both swimming tests were conducted at an actuation frequency of 0.33 Hz (2 s contraction and 1 s relaxation). The successful variation of swimming directions shows that KryptoJelly has the potential to be an essential tool in underwater exploration.

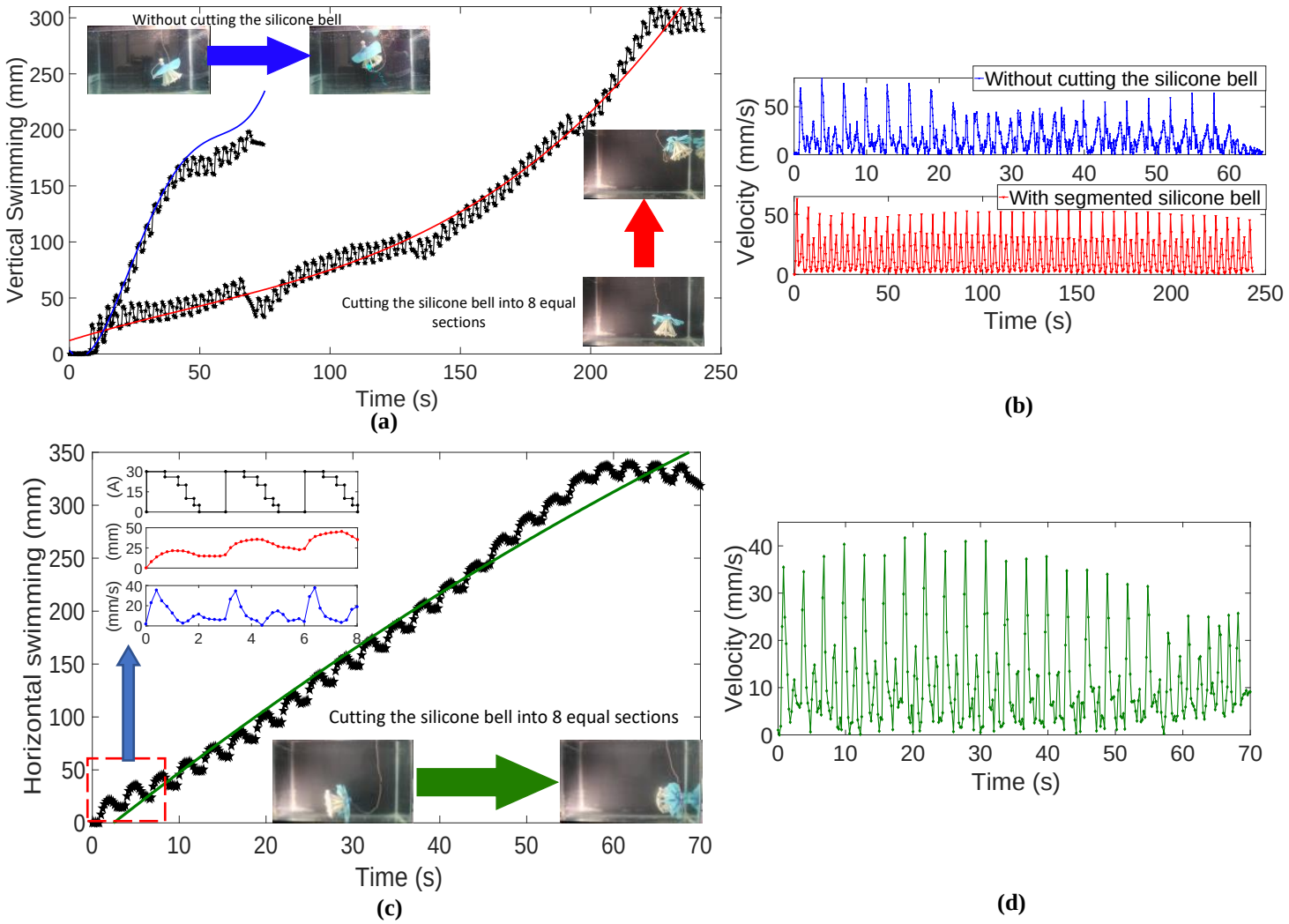

Figure 6. Underwater swimming analysis: (a) comparison of KryptoJelly swimming vertically with segmented and unsegmented bell, (b) vertical swimming instantaneous velocity with segmented and unsegmented bell, (c) horizontal swimming, and (d) horizontal swimming velocity.

3.4. Untethered actuation and operation duration

The purpose of this paper is to present the swimming characterization of a jellyfish robot actuated by shape memory alloys that are configured and housed in a 3D printed structure. We demonstrated swimming characteristics using an external DC power supply. Here, we show the potential of using untethered swimming. To this end, a circuit was designed to fit inside a casing that is inserted under the jellyfish structure as shown in figure 7 (a). The circuit consists of an Arduino micro controller, Bluetooth communication module (HC-05), a relay switch, and NiMH rechargeable battery. The battery can supply 8.4V for in air actuation and 25V for underwater actuation; it has 30A output current capabilities. A snapshot and detailed circuit diagram is provided in figure 7 (b and c). Three NiMH 4.5Ah (37.8Wh) batteries connected in series (total 25V) are used to power the SMA actuators. Figure 7 (d) show the snapshot of the KryptoJelly flapping for both unsegmented (left) and segmented (right) bell using the circuit design provided (located outside the fish tank) also provided in supplementary Movie 4. With this configuration, KryptoJelly can operate up to 10 minutes underwater before the flapping strain is decreased due to the battery's charge. This test indicates that the robot can be powered wirelessly using rechargeable battery. We realized that more work needs to be performed to

make it fully untethered but the main ideas presented in this paper are the one highlighted at the beginning of this paper.

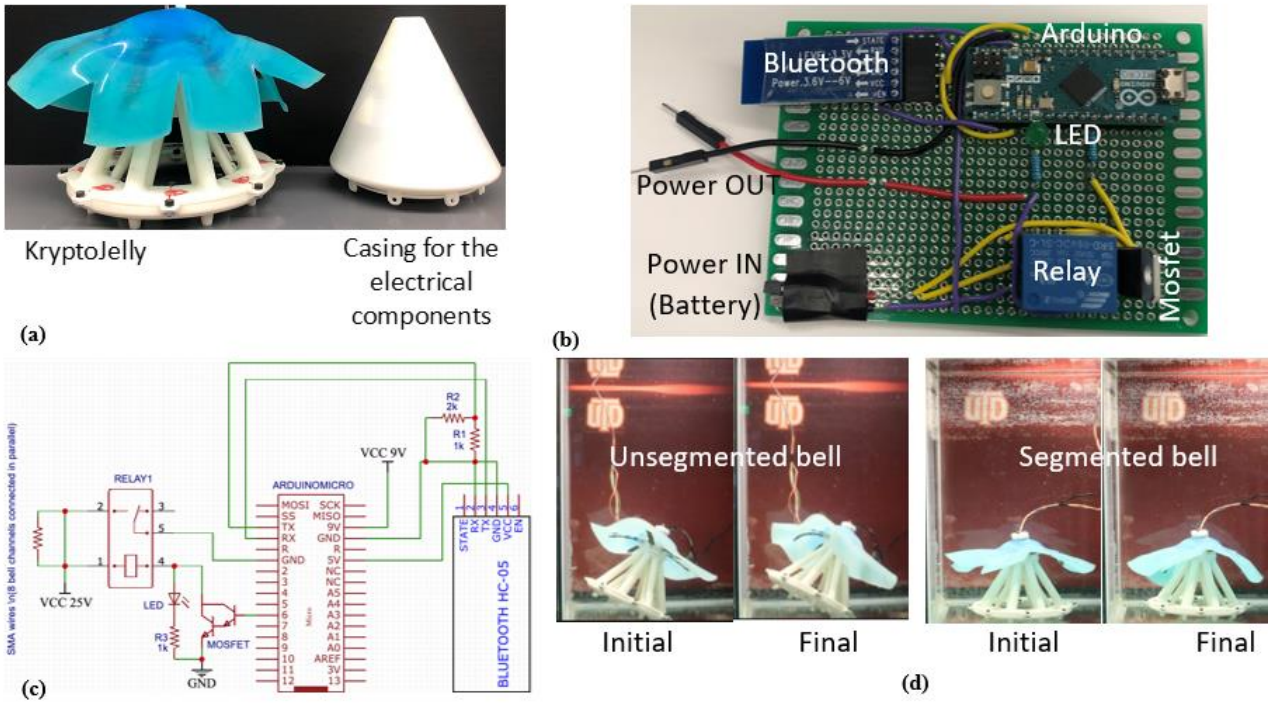

Figure 7: Design for untethering powering of KryptoJelly: (a) Assembled KryptoJelly (left) and 3D printed power casing (right), (b) electrical components used to power KryptoJelly for untethered swimming, (c) circuit schematic diagram and, (d) testing flapping of the bell.

4. Conclusion and Future Work

This paper presented a multidirectional underwater swimming jellyfish robot, along with the design and fabrication of the 3D printed body and soft silicone bell of 210 mm diameter. The muscle integration process is simple and highly repeatable. KryptoJelly is shown carrying its own weight almost 650g using eight sets of actuators each weighing 14 mg (~6000 times the total mass of the actuators), swimming vertically at instantaneous speed up to 60 mm/s for the unsegmented bell and 51 mm/s for the segmented bell. The robot was also able to swim horizontal distances at an instantaneous speed of 45 mm/s. Comprehensive underwater characterization of the SMA actuator with a length of 95 mm and a diameter of 127 µm (single wire) under varying parameters such as input power and pre-stress is also demonstrated in this paper. The actuator characterization showed that the optimal pre-stress is at 300 g and the best actuation is achieved at the 5-step power input. The increase in input energy results in a strain actuation of almost 5% at a frequency of 0.33Hz. Actuating SMA in water plays a vital role to rapidly cool the actuators and maintaining asymmetric strain. The lifecycle test showed that KryptoJelly will be able to operate up to 1 hour and 33 minutes (1608 cycles) in the water while directly connected to an external power supply. A circuit is also developed and tested to show the potential of untethered wireless powering and control of KryptoJelly. A rigid capsule that can easily fit under the robot was 3D printed for carrying the battery and circuit. The presented powering unit has the capacity to operate the KryptoJelly continuously for a duration of 10 minutes. A close-up view of the robot while the bell is in a relaxed position and contracted state are shown in Figure 8 (Movie 2). Future work will include further testing of the robot with an onboard circuit to study the untethered swimming capabilities using a battery. Adding devices and sensors such as a thermal imaging camera, pressure sensor, and sonar mapping sensor will be greatly beneficial for tasks such as underwater exploration and mapping.

Figure 8: Snapshots of the close-up views of KryptoJelly when the bell is relaxed (left) and when it is contracted and moving vertically (right).

Acknowledgments

The authors would like to thank Arye Levi for his help during the initial work of this study.

AUTHORS CONTRIBUTION

Y.A., M.P., N.M., designed the robot. Y.A., M.P., N.M., contributed to experimental results and analysis of the swimming experiments and analysis. Y.A., M.P, A.H conducted the lifecycle testing and analysis and SMA characterization. Y.T. conceived the idea of the robot, bioinspiration and led the project. All authors conceived the experimental work, wrote the paper, and provided feedback.

FUNDING

The authors would like to acknowledge the support of the Office of Naval Research (ONR), Young Investigator Program, under Grant No. N00014-15-1-2503. We would like to thank Dr. McKenna, the program manager at ONR Biorobotics program.

SUPPLEMENTARY MATERIALS

Movie S1. Purple striped jellyfish swimming. Shot by Armita Hamidi at Monterey Bay Aquarium. https://youtu.be/vCoFwVLh5ps

Movie S2. Fast camera video (capture rate of 100Hz) of vertical swimming for segmented jellyfish utilizing the 5-step power input at an actuation rate of 0.33Hz.
https://youtu.be/WK5S93YHb9w

Movie S3. Horizontal swimming of segmented bell jellyfish utilizing the 5-Step power input at an actuation rate 0.33Hz.
https://youtu.be/oy-MlXz6j1M

Movie S4: Battery powered actuation of Kryptojelly.
https://youtu.be/uVeHZr3UsZU

References

1. Yirmibeşoğlu, O.D., Oshiro, T. T., Olson, G., Palmer, C., & Mengüç, Y., *Evaluation of 3D Printed Soft Robots in Radiation Environments and Comparison With Molded Counterparts.* Frontiers in Robotics and AI, 2019. **6**: p. 40.
2. Schmitt, F., Piccin, O., Barbé, L., & Bayle, B., *Soft Robots Manufacturing: A Review.* Frontiers in Robotics and AI, 2018. **5**: p. 84.
3. Colin, S.P. and J.H. Costello, *Morphology, swimming performance and propulsive mode of six co-occurring hydromedusae.* Journal of experimental biology, 2002. **205**(3): p. 427-437.
4. Colin, S.P., J.H. Costello, J.O. Dabiri, A. Villanueva, J.B. Blottman, B.J. Gemmell, and S. Priya, *Biomimetic and Live Medusae Reveal the Mechanistic Advantages of a Flexible Bell Margin.* Plos One, 2012. **7**(11).
5. Gong, Z., Chen, B., Liu, J., Fang, X., Liu, Z., Wang, T., & Wen, L., *An Opposite-Bending-and-Extension Soft Robotic Manipulator for Delicate Grasping in Shallow Water.* Frontiers in Robotics and AI, 2019. **6**: p. 26.
6. Almubarak, Y. and Y. Tadesse, *Twisted and coiled polymer (TCP) muscles embedded in silicone elastomer for use in soft robot.* International Journal of Intelligent Robotics and Applications, 2017. **1**(3): p. 352-368.
7. Villanueva, A., C. Smith, and S. Priya, *A biomimetic robotic jellyfish (Robojelly) actuated by shape memory alloy composite actuators.* Bioinspiration & biomimetics, 2011. **6**(3): p. 036004.
8. Katzschmann, R.K., J. DelPreto, R. MacCurdy, and D. Rus, *Exploration of underwater life with an acoustically controlled soft robotic fish.* 2018.
9. Mather, J.A., *How do octopuses use their arms?* Journal of Comparative Psychology, 1998. **112**(3): p. 306.
10. Wu, L., I. Chauhan, and Y. Tadesse, *A Novel Soft Actuator for the Musculoskeletal System.* Advanced Materials Technologies, 2018. **3**(5): p. 1700359.
11. Vogel, V., *Soft robotics: bionic jellyfish.* Nature materials, 2012. **11**(10): p. 841.
12. Wang, Z., G. Hang, J. Li, Y. Wang, and K. Xiao, *A micro-robot fish with embedded SMA wire actuated flexible biomimetic fin.* Sensors and Actuators A: Physical, 2008. **144**(2): p. 354-360.
13. Low, K.H., J. Yang, A.P. Pattathil, and Y. Zhang. *Initial prototype design and investigation of an undulating body by SMA*. in *2006 IEEE International Conference on Automation Science and Engineering*. 2006. IEEE.
14. Tadesse, Y., A. Villanueva, C. Haines, D. Novitski, R. Baughman, and S. Priya, *Hydrogen-fuel-powered bell segments of biomimetic jellyfish.* Smart Materials and Structures, 2012. **21**(4): p. 045013.

15. Yeom, S.-W. and I.-K. Oh, *A biomimetic jellyfish robot based on ionic polymer metal composite actuators.* Smart materials and structures, 2009. **18**(8): p. 085002.
16. Frame, J., N. Lopez, O. Curet, and E.D. Engeberg, *Thrust force characterization of free-swimming soft robotic jellyfish.* Bioinspiration & biomimetics, 2018. **13**(6): p. 064001.
17. Alejandre, A., O. Olszewski, and N. Jackson. *Actuation control of a PiezoMEMS biomimetic robotic jellyfish*. in *Smart Sensors, Actuators, and MEMS VIII*. 2017. International Society for Optics and Photonics.
18. Cheng, T., G. Li, Y. Liang, M. Zhang, B. Liu, T.-W. Wong, J. Forman, M. Chen, G. Wang, and Y. Tao, *Untethered soft robotic jellyfish.* Smart Materials and Structures, 2018. **28**(1): p. 015019.
19. Marut, K., C. Stewart, T. Michael, A. Villanueva, and S. Priya, *A jellyfish-inspired jet propulsion robot actuated by an iris mechanism.* Smart Materials and Structures, 2013. **22**(9): p. 094021.
20. Joshi, A., A. Kulkarni, and Y. Tadesse, *FludoJelly: Experimental Study on Jellyfish-Like Soft Robot Enabled by Soft Pneumatic Composite (SPC).* Robotics, 2019. **8**(3): p. 56.
21. Godaba, H., J. Li, Y. Wang, and J. Zhu, *A soft jellyfish robot driven by a dielectric elastomer actuator.* IEEE Robotics and Automation Letters, 2016. **1**(2): p. 624-631.
22. Kazemi-Lari, M.A., A.D. Dostine, J. Zhang, A.S. Wineman, and J.A. Shaw. *Robotic jellyfish actuated with a shape memory alloy spring*. in *Bioinspiration, Biomimetics, and Bioreplication IX*. 2019. International Society for Optics and Photonics.
23. Zhou, Y., H. Jin, C. Liu, E. Dong, M. Xu, and J. Yang. *A novel biomimetic jellyfish robot based on a soft and smart modular structure (SMS)*. in *2016 IEEE International Conference on Robotics and Biomimetics (ROBIO)*. 2016. IEEE.
24. Wilbur, C., W. Vorus, and Y. Cao, *14 A Lamprey-Based Undulatory Vehicle.* Neurotechnology for biomimetic robots, 2002: p. 285.
25. Chen, Z., T.I. Um, and H. Bart-Smith, *A novel fabrication of ionic polymer–metal composite membrane actuator capable of 3-dimensional kinematic motions.* Sensors and Actuators A: Physical, 2011. **168**(1): p. 131-139.
26. Aureli, M., V. Kopman, and M. Porfiri, *Free-locomotion of underwater vehicles actuated by ionic polymer metal composites.* IEEE/ASME transactions on mechatronics, 2010. **15**(4): p. 603-614.
27. Phamduy, P., M.A. Vazquez, C. Kim, V. Mwaffo, A. Rizzo, and M. Porfiri, *Design and characterization of a miniature free-swimming robotic fish based on multi-material 3D printing.* International Journal of Intelligent Robotics and Applications, 2017. **1**(2): p. 209-223.
28. Chu, W.-S., K.-T. Lee, S.-H. Song, M.-W. Han, J.-Y. Lee, H.-S. Kim, M.-S. Kim, Y.-J. Park, K.-J. Cho, and S.-H. Ahn, *Review of biomimetic underwater robots using smart actuators.* International journal of precision engineering and manufacturing, 2012. **13**(7): p. 1281-1292.
29. Salazar, R., A. Campos, V. Fuentes, and A. Abdelkefi, *A review on the modeling, materials, and actuators of aquatic unmanned vehicles.* Ocean Engineering, 2019. **172**: p. 257-285.
30. Salazar, R., V. Fuentes, and A. Abdelkefi, *Classification of biological and bioinspired aquatic systems: A review.* Ocean Engineering, 2018. **148**: p. 75-114.

31. Tadesse, Y., N. Thayer, and S. Priya, *Tailoring the response time of shape memory alloy wires through active cooling and pre-stress.* Journal of Intelligent Material Systems and Structures, 2010. **21**(1): p. 19-40.
32. Lee, H.T., M.S. Kim, G.Y. Lee, C.S. Kim, and S.N. Ahn, *Shape Memory Alloy (SMA)-Based Microscale Actuators with 60% Deformation Rate and 1.6 kHz Actuation Speed.* Small, 2018. **14**(23).
33. Furst, S.J. and S. Seelecke, *Modeling and experimental characterization of the stress, strain, and resistance of shape memory alloy actuator wires with controlled power input.* Journal of Intelligent Material Systems and Structures, 2012. **23**(11): p. 1233-1247.
34. Song, S.H., J.Y. Lee, H. Rodrigue, I.S. Choi, Y.J. Kang, and S.H. Ahn, *35 Hz shape memory alloy actuator with bending-twisting mode.* Scientific Reports, 2016. **6**.
35. Konh, B., S. Karimi, and S. Miller. *Feasibility study of an active soft catheter actuated by SMA wires*. in *Smart Structures and NDE for Industry 4.0*. 2018. International Society for Optics and Photonics.
36. Wu, L., M.J. de Andrade, L.K. Saharan, R.S. Rome, R.H. Baughman, and Y. Tadesse, *Compact and low-cost humanoid hand powered by nylon artificial muscles.* Bioinspiration & biomimetics, 2017. **12**(2): p. 026004.
37. Saharan, L. and Y. Tadesse. *Robotic hand with locking mechanism using TCP muscles for applications in prosthetic hand and humanoids*. in *Bioinspiration, Biomimetics, and Bioreplication 2016*. 2016. International Society for Optics and Photonics.
38. Leo, D.J., *Engineering Analysis of Smart Material Systems*. Vol. 1st Edition. 2007, Hoboken, New Jersey USA: John Wiley and sons Inc.
39. Dynalloy.Inc. *Technical Characteristics of Flexinol*.
40. Lagoudas, D., D. Miller, L. Rong, and P. Kumar, *Thermomechanical fatigue of shape memory alloys.* Smart Materials and Structures, 2009. **18**(8): p. 085021.
41. Zhang, Y.H., Y.J. You, Z. Moumni, G. Anlas, J.H. Zhu, and W.H. Zhang, *Experimental and theoretical investigation of the frequency effect on low cycle fatigue of shape memory alloys.* International Journal of Plasticity, 2017. **90**: p. 1-30.
42. Maletta, C., E. Sgambitterra, F. Furgiuele, R. Casati, and A. Tuissi, *Fatigue properties of a pseudoelastic NiTi alloy: Strain ratcheting and hysteresis under cyclic tensile loading.* International Journal of Fatigue, 2014. **66**: p. 78-85.
43. Calhoun, C., R. Wheeler, T. Baxevanis, and D. Lagoudas, *Actuation fatigue life prediction of shape memory alloys under the constant-stress loading condition.* Scripta Materialia, 2015. **95**: p. 58-61.
44. Smith, K.N., *A stress-strain function for the fatigue of metals.* Journal of materials, 1970. **5**: p. 767-778.